Continuous and lurching traveling pulses in neuronal networks with delay and spatially decaying connectivity

David Golomb*† and G. Bard Ermentrout‡

*Zlotowski Center for Neuroscience and Department of Physiology, Faculty of Health Sciences, Ben-Gurion University of the Negev, Beer-Sheva 84105, Israel; and ‡Department of Mathematics, University of Pittsburgh, Pittsburgh, PA 15260

Edited by Nancy J. Kopell, Boston University, Boston, MA, and approved August 20, 1999 (received for review May 18, 1999)

Propagation of discharges in cortical and thalamic systems, which is used as a probe for examining network circuitry, is studied by constructing a one-dimensional model of integrate-and-fire neurons that are coupled by excitatory synapses with delay. Each neuron fires only one spike. The velocity and stability of propagating continuous pulses are calculated analytically. Above a certain critical value of the constant delay, these pulses lose stability. Instead, lurching pulses propagate with discontinuous and periodic spatio-temporal characteristics. The parameter regime for which lurching occurs is strongly affected by the footprint (connectivity) shape; bistability may occur with a square footprint shape but not with an exponential footprint shape. For strong synaptic coupling, the velocity of both continuous and lurching pulses increases logarithmically with the synaptic coupling strength g_{syn} for an exponential footprint shape, and it is bounded for a step footprint shape. We conclude that the differences in velocity and shape between the front of thalamic spindle waves *in vitro* and cortical paroxysmal discharges stem from their different effective delay; in thalamic networks, large effective delay between inhibitory neurons arises from their effective interaction via the excitatory cells which display postinhibitory rebound.

neocortex | thalamus | discharge | pulse | lurching

Neuronal population discharges appear in disinhibited coronal neocortical slices in response to electrical stimulation above a certain threshold. These slice preparations were developed initially as experimental models for epilepsy (1, 2). Recently, experimental and theoretical investigations (3–7) have tried to relate the dynamics of propagating discharge to the underlying neuronal circuitry, and to use the dynamics of cortical slices as a first stage toward understanding spatio-temporal dynamics in neuronal networks (8–10). The average discharge velocity is about 10–15 cm/s (3); neurons are recruited to the wave because of the excitatory recurrent interactions between neurons. Numerical simulations of a conductance based neuronal model with homogeneous architecture reveal that the discharge propagates at a constant velocity, as a *continuous* traveling pulse (3, 6, 7). Spatial inhomogeneities in the velocity, which were discovered experimentally, were attributed to spatial fluctuations in the synaptic and intrinsic neuronal properties along the slice (11, 12). In both theory and experiment, there was a minimal velocity below which the discharge could not propagate. Propagating discharges with similar properties and velocities have been found in other cortical structures, such as the hippocampus (13, 14) and the piriform cortex (15).

Another example of propagating discharges is the spindle-like discharges in thalamic slices (16, 17). The circuit is composed of excitatory thalamocortical (TC) cells and inhibitory reticular (RE) thalamic cells, coupled with reciprocal synaptic connections. The excitatory cells possess a postinhibitory rebound mechanism (see, e.g., ref. 18). The propagation velocity is around 1 mm/s (19). Numerical simulations have indicated that these discharges propagate in a nonsmooth, periodic, ''lurching'' manner (20, 21). Each recruitment cycle has two stages. At the first stage, a new group of inhibitory RE cells is excited by synapses from TC cells, and this RE group inhibits a new group of silent TC cells. At the second stage, the newly recruited TC cells rebound from hyperpolarization and fire a burst of action potentials. These bursts further recruit more RE cells during the next cycle. Thus, the lurching wave has a periodic nature at the front. Rinzel *et al*. (22) have reduced the model of a thalamic slice to a model of coupled inhibitory units and found that the model can also exhibit lurching waves if the synaptic reversal potential is hyperpolarized enough. With off-center (coupling that is zero at zero distance and has a maximum at a finite distance) inhibition, lurching waves can propagate in one direction while continuous waves can propagate in the other direction, demonstrating bistability[§] in the system. An experimental *in vivo* study suggested that the RE nucleus may generate spindle-like oscillations (23). Numerical simulations of isolated RE networks showed that such oscillations can propagate as lurching pulses (20) or as continuous pulses (24).

In this work, we explore the recruitment stage of these two propagating discharges. We ask the following questions.

1. What is the basis for the different types (continuous or lurching) of propagating discharges? How is the type determined by the network architecture, the kinetics of single cells and synapses, and the synaptic delay?
2. What is the relationship between the velocity of the pulse (or wave), and the intrinsic, synaptic, and architecture properties of the system?

Specifically, we want to know why cortical networks exhibit fast, continuous discharges, whereas thalamic networks exhibit slow, lurching discharges. To answer these questions, we develop a joint conceptual framework for the two types of networks, which enables us to compare the two preparations and the two types of discharge propagation. We show that under certain conditions and approximations, the discharge dynamics of both cortical and thalamic slices can be reduced to a model of integrate and fire neurons in which each neuron can fire only one spike. Neurons are coupled by excitatory synapses with delay, which is small for cortical networks and large for thalamic networks. Using analytical and numerical methods, we find that continuous pulses exist and are stable for small values of constant (space-independent) delay. As the constant delay in-

This paper was submitted directly (Track II) to the PNAS office.

Abbreviations: TC, thalamocortical; RE, reticular; EPSC, excitatory postsynaptic conductance.

†To whom reprint requests should be addressed at: Department of Physiology, Faculty of Health Sciences, P.O.B. 653, Ben-Gurion University of the Negev, Beer-Sheva 84105, Israel. E-mail: golomb@bgumail.bgu.ac.il.

§The word "bistability" is used here in a broad sense, despite the fact that the system dynamics do not converge to an attractor.

The publication costs of this article were defrayed in part by page charge payment. This article must therefore be hereby marked "*advertisement*" in accordance with 18 U.S.C. §1734 solely to indicate this fact.

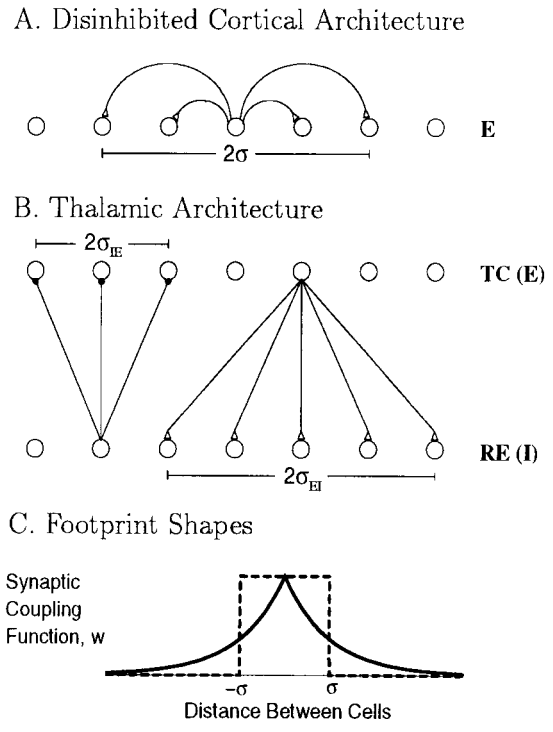

Fig. 1. (*A*) Synaptic architecture of the cortical and thalamic models. Both have a one-dimensional architecture, with the coupling between cells decaying with their distance. The footprint lengths are denoted by σ (3, 20). In the case of two populations, the first and second letters in the subscript denote the pre- and postsynaptic populations respectively. (*A*) Disinhibited cortical model: a chain of excitatory (E) cells. (*B*) Thalamic model. Inhibitory (I) RE cells inhibit excitatory (E) TC cells, and TC cells excite RE cells. Mutual inhibition between RE cells is neglected because it has relatively small effect on discharge propagation (16, 19). (*C*) Exponential (solid line) and square (dashed line) footprint shapes.

creases, this pulse loses stability and lurching pulses are obtained.

The Model

Reduction of Models of Paroxysmal Discharges in Disinhibited Cortical Networks. Simulations of a conductance-based models of paroxysmal discharges in disinhibited cortical tissues (Fig. 1*A*) reveal that the discharge velocity v is determined primarily by the response of the postsynaptic neuron to the first one or two spikes of the presynaptic neuron (3), especially with prominent synaptic depression. Therefore, taking only the first spike of each presynaptic neuron into account and ignoring all the others is a good approximation (6). For example, if we assume that only the first spike elicits an excitatory postsynaptic conductance (EPSC) for the parameters of figure 8 in ref. 3, the velocity decreases by only 15%.

Even adjacent cortical neurons have a delay of about 2 ms (25, 26); more distant neurons are expected to have a larger delay because of the finite axonal connectivity. The delay τ_{delay} between neurons at positions x and x' is therefore

$$\tau_{\text{delay}} = \tau_d + \frac{x - x'}{c}, \qquad [1]$$

where τ_d is the constant delay and c is the axonal conduction velocity.

Reduction of Models of Spindle-Like Discharges in Thalamic Networks. In this paper, we consider a spatially structured network of excitatory neurons, which may be interpreted as a reduction from a two-population thalamic network (Fig. 1*B*). The idea is that because the RE-to-TC projection is topographic and acts via $GABA_A$ and $GABA_B$ receptors, excitation of one RE cell would result in a delayed barrage of EPSCs in the neighboring RE cells through the disynaptic RE-TC-RE loop. In this idealized view of the isolated thalamic circuit, the RE cell layer acts effectively as a cell population with reciprocal AMPA-mediated excitatory interactions, with an effective delay τ_d (Eq. **1**) of order 100 ms caused by the time needed for the TC cell to rebound from inhibition. Because we are interested in this work only in the recruitment process, we can model the system by considering only the first "spike" each cell fires. The large effective delay ensures that the velocity at moderate coupling is determined mainly by the first spike. This spike represents a Ca^{2+} spike upon which rides a train of action potentials (20). The assumption of fixed effective delay only applies if those TC cells that receive inhibitory input are in burst-capable mode.

Model Description. We use the integrate-and-fire model (6, 27)

$$\frac{\partial V(x,t)}{\partial t} = -\frac{V(x,t)}{\tau_0} + I_{\text{syn}}(x,t) + I_{\text{app}}(x,t) \qquad [2]$$

for $0 < V(x,t) < V_T$, where $V(x,t)$ is the membrane potential of a neuron at a position x and time t, τ_0 is the passive membrane time constant of the neuron, I_{syn} is the normalized synaptic input, and I_{app} is the normalized applied current; $I_{\text{app}} = 0$ unless stated differently. When V of a neuron reaches the threshold V_T at time $T(x)$, the neuron fires a spike, and cannot fire more spikes afterwards; its voltage is set to zero at later times. We assume that the number of neurons within a footprint length is large and therefore use a continuum model and replace the sum over the presynaptic neurons by an integral:

$$I_{\text{syn}}(x,t) = g_{\text{syn}} \int_{-\infty}^{\infty} dx' w(x - x') \alpha[t - T(x') - \tau_{\text{delay}}], \qquad [3]$$

where $g_{\text{syn}} = \tilde{g}_{\text{syn}}\Delta/C$, $\tilde{g}_{\text{syn}}$ is the synaptic conductance, C is the membrane capacitance, and $\Delta = V - V_{\text{syn}}$ is approximated here to be a constant ("coupling by currents", see, e.g., refs. 6 and 28); τ_{delay} is the delay between the post- and presynaptic neurons. The temporal shape of the EPSC that a postsynaptic cell at a position x receives following a spike of a presynaptic cell at a position x' is given by the normalized α function $\alpha[t - T(x')]$:

$$\alpha(t) = \begin{cases} \dfrac{e^{-t/\tau_1} - e^{-t/\tau_2}}{\tau_1 - \tau_2} & t \geq 0 \\ 0 & \text{otherwise} \end{cases}, \qquad [4]$$

where τ_1 and τ_2 are the synaptic rise and decay time, respectively. The spatial dependence of the synaptic strength on the distance between neurons, $w(x)$, is called the "synaptic footprint shape" (3, 20). We examine two shapes (Fig. 1*C*):

$$w(x) = \frac{1}{2\sigma} e^{-|x|/\sigma} \quad \text{Exponential.} \qquad [5]$$

$$w(x) = \begin{cases} \dfrac{1}{2\sigma} & |x| \leq \sigma \\ 0 & |x| > \sigma \end{cases} \quad \text{Square.} \qquad [6]$$

σ is called the "synaptic footprint length."

Define the response (Green's) function $G(t)$ for $t > 0$ as

$$\frac{dG}{dt} = -\frac{G}{\tau_0} + \alpha(t);\ G(0) = 0 \qquad [7]$$

and $G(t) = 0$ for $t < 0$. Then, for $\tau_1 = 0$,

$$G(t) = \begin{cases} \dfrac{\tau_0}{\tau_0 - \tau_2}\,(e^{-t/\tau_0} - e^{-t/\tau_2}) & t \geq 0 \\ 0 & \text{otherwise} \end{cases} \qquad [8]$$

for $t > 0$. The function G is the normalized EPSP (excitatory postsynaptic potential) developed in the cell as a response to the EPSC (Eq. **4**). The Volterra representation of Eqs. **2** and **3** for neurons that can fire only one spike is

$$\frac{V_T}{g_{\text{syn}}} = \int_{-\infty}^{\infty} dx' w(x') G\left[T(x) - T(x - x') - \tau_d - \frac{x'}{c} \right] \qquad [9]$$

together with the condition that $T(x)$ is the first time that the voltage crosses the threshold. This condition requires that

$$\frac{dV[x, T(x)]}{dt} > 0. \qquad [10]$$

Numerical Methods. Eqs. **2** and **3** are simulated numerically by discretizing space. There are N neurons in the chain, and the density of neurons is ρ per length σ. The coupled system of ordinary differential equations for the integrate-and-fire neurons is solved by using exact integration (29). To stimulate the network, applied current is "injected" into a group of neurons on the "left" of the system (small x values) that span a length at least equal to the footprint length σ ("shock" initial conditions).

Results

In the following, we calculate the existence and stability regimes and the velocity of the continuous and lurching pulses for $c \to \infty$ (infinite axonal conduction velocity). The effect of finite axonal velocity c is reported at the end of this section. In most calculations we will take $\tau_1 = 0$ for simplicity, unless stated otherwise. Details of the analytical calculations will be published elsewhere.

Continuous and Lurching Pulses. A pulse can propagate along the network in response to "shock" initial conditions. For zero or small τ_d (below a critical value τ_{dc}), the pulse is continuous far from the stimulus region (Fig. 2*A*), and the firing times of the neurons obey $T(x) = T_0 + x/\nu$, where ν is the pulse velocity and T_0 is an arbitrary time. The neuronal potential satisfies a traveling pulse equation as well: $V(x, t) = \bar{V}(x - \nu t)$ (3, 6, 7). For large τ_d (above τ_{dc}), a lurching propagating pulse is observed (Fig. 2*B*). Space is spontaneously segregated into basic spatial units, each with a spatial period length L, and the firing time in each unit can be obtained from the spatial period in the previous unit according to

$$T(x + L) = T(x) + T_{\text{per}}. \qquad [11]$$

The average velocity of the pulse is $\nu = L/T_{\text{per}}$. One can easily show that the function $T(x) - x/\nu$ is a periodic function with a period L, as demonstrated in Fig. 2*C*.

Existence, Stability, and Velocity of Continuous Pulses. *General formalism.* Substituting the condition for a continuous pulse, $T(x) = x/\nu$, into the evolution Eq. **9**, we obtain

$$\int_0^{\infty} dy w(y + \tau_d \nu) G(y/\nu) = V_T/g_{\text{syn}} \qquad [12]$$

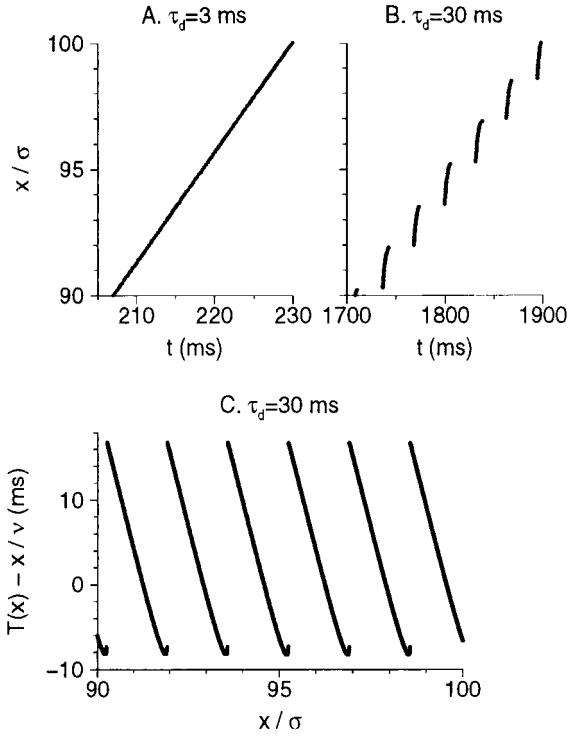

Fig. 2. (*A* and *B*) Rastergrams obtained from simulating Eqs. **2**, **3**, and **5** with the condition that each neuron can fire only one spike. Parameters: $\tau_0 = 30$ ms, $\tau_2 = 2$ ms, $g_{\text{syn}}V_T = 10$, $c \to \infty$, $N = 5 \times 10^4$, $\rho = 500$; for these parameters, $\tau_{dc} = 11.15$ ms. The solid circles represent the firing time of neurons as a function of their normalized position x/σ; spikes of only one out of every 50 neuron are plotted. Together, the groups of solid circles looks almost like one continuous line. (*A*) For $\tau_d < \tau_{dc}$ (3 ms), a continuous pulse is obtained. (*B*) For $\tau_d > \tau_{dc}$ (30 ms), the pulse is lurching. (*C*) The fluctuation around the constant-velocity solutions, $T(x) - x/\nu$ are plotted as a function of position x/σ for the same parameters as in *B*, to demonstrate the oscillatory nature of the lurching pulse. The firing times of all the neurons are plotted here as solid dots.

together with the condition (a consequence of Eq. **10**)

$$d\nu/dg_{\text{syn}} > 0. \qquad [13]$$

Stability of the continuous pulse is calculated by analyzing spatial perturbation of Eq. **9** (see also ref. 7).

Exponential footprint shape. The velocity ν is determined using Eqs. **5**, **8**, and **12**:

$$\frac{(\tau_0\nu + \sigma)(\tau_2\nu + \sigma)}{\tau_0\nu\sigma} \exp\left(\frac{\tau_d\nu}{\sigma}\right) = \frac{g_{\text{syn}}}{2V_T} \qquad [14]$$

together with Eq. **13**; this is an extension of the equation obtained in ref. 6 for $\tau_d = 0$. From this equation, one can see the following:

1. For $\tau_d = 0$, the left-hand-side of Eq. **14** has a minimum with respect to ν at $\nu_{\min} = \sigma/\sqrt{\tau_0\tau_2}$. Continuous pulses cannot propagate[¶] with velocity smaller than $\nu_{\min}$, which is obtained for a minimal synaptic coupling $g_{\text{syn,min}}$.
2. Because $\exp(\tau_d\nu/\sigma) > 1$ and increases with τ_d, $\nu_{\min}$ decreases with τ_d and is obtained for larger $g_{\text{syn,min}}$.
3. For $\tau_d > 0$ and at large enough g_{syn}, the velocity is determined mainly by the exponential factor in Eq. **14** and therefore

[¶]For $g_{\text{syn}} > g_{\text{syn,min}}$, there are two branches of solutions to Eq. **14**. At the slow branch, ν decreases with g_{syn} (3, 6), and therefore this solution is not meaningful.

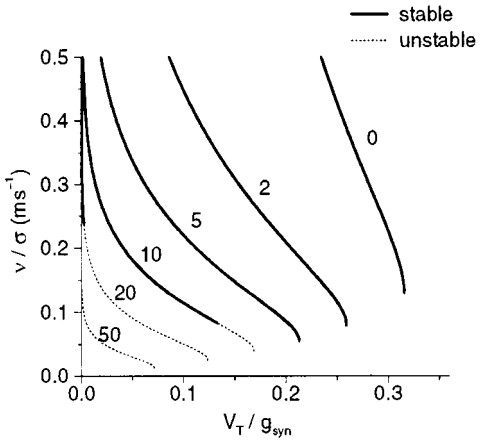

Fig. 3. The velocity of the continuous pulse as a function of V_T/g_{syn} for several values of τ_d and exponential footprint shape (Eq. **14**). The wide lines represent stable pulses and the narrow lines represent unstable pulses. The number above each line, from 0 to 50, denotes the value of τ_d. Parameters: $\tau_0 = 30$ ms, $\tau_2 = 2$ ms.

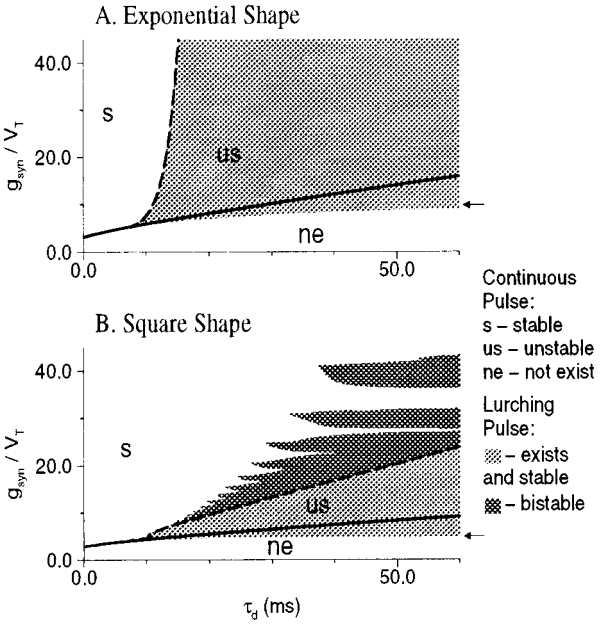

Fig. 4. Regimes of existence and stability of the continuous and lurching pulses in the τ_d-ν plane are shown in *A* for exponential footprint shape and in *B* for square footprint shape. Parameters are as in Fig 3. The boundaries of the regime in which the lurching pulse exists and is stable were computed from numerical simulations, in which a pulse was initiated by a ''shock'' initial stimulus; $N = 20{,}000$, $\rho = 50$. The solid line denotes the minimal possible velocity as a function of g_{syn}; the continuous pulse becomes unstable (via a Hopf bifurcation) on the dashed line. The continuous pulse is therefore stable above both the solid and long dashed line, as denoted by ''s.'' It is unstable between the two lines, as denoted by ''us,'' and does not exist below the continuous line, as denoted by ''ne.'' The light-gray shading represents the region for which lurching pulses (and not continuous pulses) are obtained. Bistable regimes, in which the continuous pulse can coexist with the lurching pulse, are denoted by the dark-gray shading. For the square footprint shape (*B*), but not for the exponential footprint shape, there is such a bistable regime that has a ''tongue-like'' structure. The arrow at the right of each graph represents the minimal values of g_{syn} for which the lurching pulse is found in simulations for $\tau_d \to \infty$.

depends logarithmically on g_{syn} to the highest order. In contrast, for $\tau_d = 0$, the velocity exhibits a power-law dependence on g_{syn} at large g_{syn} (6).

Graphs of ν as a function of $1/g_{syn}$ for several values of τ_d, together with results of the stability analysis of the pulses, are shown in Fig. 3. For large enough τ_d, the pulse is unstable for small g_{syn} (and low velocities). The various behavioral regimes of the continuous pulse in the $\tau_d - g_{syn}$ plane are plotted in Fig. 4*A*. Below the solid line, the continuous pulse does not exist. Above this line, the continuous pulse is stable if the delay τ_d is smaller than a critical delay τ_{dc} and is unstable otherwise. The dashed line denotes the value of τ_{dc} as a function of g_{syn}. At very large g_{syn}, τ_{dc} increases logarithmically with g_{syn}.

The boundaries of the regime of existence of lurching pulses have been located by using numerical simulations, and they are represented by the light-shaded area in Fig. 4*A*. Lurching pulses are observed in all the parameter regimes in which the continuous pulse is unstable. In addition, lurching pulses are also observed in a parameter regime in which the continuous pulse does not exist at all. At very large delay, lurching pulses are observed above a critical value of g_{syn}, denoted by the arrow, that does not depend on τ_d (see below).

Square footprint shape. The velocity ν is determined by using Eqs. **6**, **8**, and **12**:

$$\frac{2V_T}{g_{syn}} = \frac{\tau_0 \nu}{\sigma}\left\{1 - \frac{1}{\tau_0 - \tau_2}\left[\tau_0 \exp\left(\frac{\tau_d - \sigma/\nu}{\tau_0}\right) - \tau_2 \exp\left(\frac{\tau_d - \sigma/\nu}{\tau_2}\right)\right]\right\}. \quad [15]$$

The qualitative results regarding the minimal velocity and its dependence on τ_d are the same as for the exponential case. The situation is different, however, for large g_{syn}. For $\nu = \sigma/\tau_d$, the right-hand side of Eq. **15** is zero. Hence, at the limit $g_{syn} \to \infty$ the velocity of the continuous pulse approaches the finite value σ/τ_d.

The different behavioral regimes of the continuous pulse for a square footprint shape are presented in Fig. 4*B*. The critical delay τ_{dc} increases with g_{syn} almost linearly at large g_{syn}. As a result, for a specific τ_d there is a moderate g_{syn} value for which the continuous pulse is stable. Lurching pulses are obtained in the region denoted by the gray shading in Fig. 4*B*. There are two apparent differences between the situation here and the situation for exponential footprint shape. First, lurching pulses exist in an area which is composed of ''tongues.'' Second, a *bistable* regime exists, denoted by the dark-gray shading, in which the two types of pulses can propagate, depending on the initial stimulation (22).

Velocity of Lurching Pulses. How does the velocity of the lurching pulse depend on the synaptic strength? We can calculate this velocity in the case

$$\tau_2 \ll \tau_0 \ll \tau_d. \quad [16]$$

This case corresponds to a large delay and fast EPSCs (as in thalamic slices); note that $\tau_1 = 0$. Simulations of such cases show that neurons fire only during a time period that is small in comparison to the delay, and L is almost unaffected by the delay period as long as it is large enough. Therefore, the pulse velocity is $\nu = L/\tau_d$. For $\tau_d \gg \tau_0$, a neuron that fires during the nth lurching period (with length L and time T_{per}) is affected only by neurons that have fired during the previous lurching period. The contribution to the potential of that neuron of neuronal EPSCs from neurons in earlier periods has already decayed, mostly because of the large delay and also because of the fact that neuron in earlier lurching periods are more distant from that neuron. The neuron is also not affected by neurons that fire

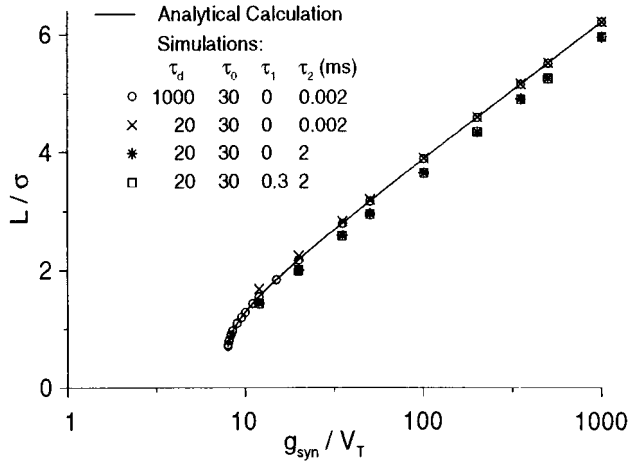

Fig. 5. The normalized length of the lurching period L/σ as a function of g_{syn}/V_T. The analytical solution for the case $\tau_1 = 0$, $\tau_2 \ll \tau_0 \ll \tau_d$ (Eq. **18**) is represented by the solid line. Simulations were carried out with $N = 200{,}000$ and $\rho = 500$. Simulations results with the corresponding parameter set: $\tau_d = 1000$ ms, $\tau_0 = 30$ ms, $\tau_1 = 0$, $\tau_2 = 0.002$ ms, denoted by ○, fit the analytical solutions almost exactly. The symbol × denotes simulations with $\tau_d = 20$ ms, $\tau_0 = 30$ ms, $\tau_1 = 0$, $\tau_2 = 0.002$ ms; the symbol ∗ denotes simulations with $\tau_d = 20$ ms, $\tau_0 = 30$ ms, $\tau_1 = 0$, $\tau_2 = 2$ ms; and the symbol □ denotes simulations with $\tau_d = 20$ ms, $\tau_0 = 30$ ms, $\tau_1 = 0.3$, $\tau_2 = 2$ ms.

during the same lurching period. We assume that the lurching wave is initiated at very large, negative x, and a lurching spatial period starts at $x = 0$. We define the function $f(x)$ on the interval $0 < x \le L$ to be $f(x) = T(x + nL) - nT_{per}$, where n is the integer part of $T(x)/T_{per}$ (or x/L). Neurons at a position $0 \le x < L$ will be affected only by neurons located in the interval $-L \le x < 0$. Eq. **9** becomes

$$\frac{V_T}{g_{syn}} = \int_{-L}^{0} dx' w(x - x') G[f(x) - f(x') + \hat{T}], \qquad [17]$$

where $\hat{T} = T_{per} - \tau_d$. This means that for a square footprint shape, $L \le \sigma$. Using an asymptotic expansion, we find that the length L for an exponential footprint shape is given, for the conditions in Eq. **16**, by

$$L = \sigma \ln 2 - \sigma \ln(1 - \sqrt{1 - 8V_T/g_{syn}}). \qquad [18]$$

For large g_{syn}, expanding this equation yields $L = \sigma \ln[g_{syn}/(2V_T)]$. Eq. **18** has a solution only if $g_{syn} > 8V_T$, and this is the synaptic conductance threshold for enabling the propagation of lurching waves under the conditions of Eq. **16**. The dependence of the lurching spatial period L (in units of σ) as a function of g_{syn}/V_T is shown in Fig. 5. The straight line in logarithmic scale shows that except for g_{syn} near the threshold, L increases logarithmically with g_{syn}. The open circles represent simulation results with $\tau_d = 1{,}000$ ms, $\tau_0 = 30$ ms, and $\tau_2 = 0.002$ ms, and they fall exactly on the analytical curve.

Using simulations, we tested the validity of the perturbation calculation when the time constants of the system do not fulfill Eq. **16** (not near the threshold). First, we reduced τ_d to 20 ms. This change has almost no effect for large g_{syn} and mildly increases L for small g_{syn}. This velocity increase can be attributed to the excitatory effect on a neuron from neurons in cycles before the immediate previous lurching cycle; it is stronger for small g_{syn} because of the shorter L. Second, we increased τ_2 to 2 ms. As a result, L decreases, because the EPSP developed in the postsynaptic cell (Eq. **7**) is smaller as a result of the interplay between the EPSC and the leaky neuronal integrator. This change of τ_2 has, however, an effect of less then 10% on L in comparison to the analytic result (Eq. **18**). Third, we simulated a network with $\tau_1 = 0.3$ ms. This change did not change L significantly in comparison to the case $\tau_1 = 0$. These results show that our analytical theory yields a good approximation even beyond the parameter regime for which it is derived.

Finite Axonal Velocity. When the axonal velocity c is finite, we find that the pulse velocity ν is given by the equation $1/\nu = 1/\nu_\infty + 1/c$, where ν_∞ is the pulse velocity for infinite axonal velocity. The value of τ_{dc} for a specific value of g_{syn}, and therefore the parameter regime in which stable continuous pulses are observed, do not depend on c.

Discussion

The main results of this work are as follows: (*i*) Continuous pulses can propagate along one-dimensional neuronal networks with small constant delay τ_d, and lurching pulses with periodic characteristics can propagate with large τ_d. (*ii*) The functional dependence of the propagation velocity ν on the synaptic coupling strength g_{syn} is hardly affected by the pulse type; velocities of both continuous and lurching pulses increase logarithmically with the g_{syn} for a exponential footprint shape; they are bounded for square footprint shape (this is consistent with the heuristic argument of ref. 20). (*iii*) The footprint shape strongly affects the types of pulses that are obtained with intermediate τ_d and g_{syn}. In particular, bistability (a regime where both pulse types propagate) can occur with square footprint shape [or with an off-center shape (22)] but not with exponential shape. From these results we conclude that the difference in form and velocity between cortical and thalamic propagating discharges stems from the much larger effective delay in thalamic networks.

The instability of continuous pulses with large τ_d has been shown independently by Bressloff (7). We find that lurching pulses are obtained at these value of τ_d, and sometimes they even coexist with the continuous pulses. Traub and colleagues (13, 14) have numerically studied the velocity reduction due to finite c. We find a simple analytical formula that relates the velocity with finite c to the velocity in the limit $c \to \infty$. A heuristic argument showing that the velocity of the lurching pulse increases logarithmically with g_{syn} at large g_{syn} was presented in ref. 20 (but see also ref. 30). Here, we derive the exact relationship between the velocity and g_{syn} in the limit $\tau_2 \ll \tau_0 \ll \tau_d$, and show numerically this this result is approximately valid even well beyond this parameter regime.

In our model, we are interested in the recruitment processing of neurons into the activity. We do not deal with the period of firing and its termination. Each neuron is allowed to fire only one spike. This simplification, which allows analytical treatment of the model, is justified for cortical tissues, in particular with prominent synaptic depression, because the velocity is determined primarily by the response to the first presynaptic spike. It is justified for the thalamic network because of the large effective delay. At g_{syn} values near the threshold for lurching, however, subsequent spikes may have an effects. As a result, very low velocities can be obtained in simulations of thalamic networks (20), whereas in our model velocity cannot be smaller than a finite minimal velocity.

In this work, the thalamic network model is reduced to a network of reticular thalamic neurons coupled with effective excitation with delay. Rinzel *et al.* (22) have reduced the same network into a system of thalamocortical cells coupled by effective inhibition. The two pictures are complementary. Our reduction is exact in the limit $\sigma_{IE} \ll \sigma_{EI}$ (Fig. 1*B*), where σ_{IE} and σ_{EI} denote the inhibitory-to-excitatory and the excitatory-to-inhibitory footprint lengths, respectively, whereas the reduction

of ref. 22 is exact in the limit $\sigma_{IE} \gg \sigma_{EI}$. Experimental results and computational models indicate that the sum of these two lengths is small, of order 100 μm (20, 21), but there is yet no direct measure of each length separately (31, 32). Rinzel *et al.* (22) showed that propagation can proceed smoothly with off-center footprint shape in a parameter regime in which lurching occurs with an on-center footprint shape; in some parameter regime, the wave can lurch in one direction and propagate smoothly in the other direction, exhibiting bistability. Here we show that the parameter regime in which lurching or smooth propagation occur depends on the footprint shape. Preliminary simulations of the corresponding RE-TC network model (20) indicate that for a square footprint range there is a transition from a lurching wave to a continuous wave as the AMPA conductance increases, with possible bistability, consistent with the results of the present model; "tongue"-like structures, however, were not observed.

Our model constitutes a framework for comparing and explaining the velocity and type of pulses and waves in various tissues, whose dynamics can be reduced to that of Eqs. **2** and **3**. The main reason that thalamic spindle-like waves propagate much more slowly than paroxysmal discharges in neocortex, hippocampus, and piriform cortex is that the effective delay in the thalamic network is much larger ($\approx$100 ms in comparison to $\approx$2 ms in cortex). When inhibition is mediated by $GABA_B$ inhibition only, the time needed for a TC neuron to rebound from hyperpolarization is larger in comparison to the case when $GABA_A$ inhibition is intact; the number of Na^+ action potentials within a burst is more prolonged (16, 17), which may result in a stronger effective g_{syn}. The combined effect is that the velocity is reduced with $GABA_A$ blockade (19–21). Paroxysmal discharges propagate in disinhibited tangential slices of neocortical layer IV with a velocity which is about an order of magnitude smaller than the propagation velocity in disinhibited coronal cortical slices (33). The slow velocity is partly explained by the fact that these discharges are mediated by slow NMDA receptors (larger τ_1 and τ_2, see Eqs. **4** and **14**), but assuming that the footprint length in layer IV is small in comparison to that in layer V [which mediates mostly the propagation in coronal slices (34)] is also needed to explain the slow velocity. Measurements of the minimal velocity ν_{min} [by gradual blockade of excitatory EPSCs (3)], together with our theoretical model, should be carried out in order to estimate the footprint length in layer IV networks. The model predicts that if the effective synaptic delay or conductance strength could be manipulated experimentally, there may be a transition from continuous to lurching pulses. The values of the parameters at the transition depend on the footprint shape.

Our theory enables us to estimate the footprint length based on the critical velocity, provided that we know the footprint shape, the synaptic kinetics, and the delays τ_d and c. Experiments on synaptic plasticity reveal that the response of a neuron to the first presynaptic spike may vary (either be enhanced or be depressed) in response to artificial (35) and natural (36, 37) conditions. If indeed the global excitation g_{syn} is increased but the footprint shape remains unchanged, at least within a restricted domain, the discharge velocity in a disinhibited slice should increase but the minimal velocity ν_{min} remains unchanged. Therefore, performing such experiments can corroborate or refute theories about global synaptic enhancement or reduction.

We are thankful to C. van Vreeswijk, D. Hansel, J. Rinzel, M. J. Gutnick, and E. Barkai for helpful discussions, and to C. van Vreeswijk and D. Hansel also for careful reading of the manuscript. This research was supported by a grant from the Israel Science Foundation to D.G.; G.B.E. is funded by the National Science Foundation and the National Institute of Mental Health.

1. Gutnick, M. J., Connors, B. W. & Prince, D. A. (1982) *J. Neurophysiol.* **48,** 1321–1335.
2. Connors, B. W. (1984) *Nature (London)* **310,** 685–687.
3. Golomb, D. & Amitai, Y. (1997) *J. Neurophysiol.* **78,** 1199–1211.
4. Tsau, Y., Guan, L. & Wu, J.-Y. (1998) *J. Neurophysiol.* **80,** 978–982.
5. Golomb, D. (1998) *J. Neurophysiol.* **79,** 1–12.
6. Ermentrout, G. B. (1998) *J. Comput. Neurosci.* **5,** 191–208.
7. Bressloff, P. C. (1999) *Phys. Rev. Lett.* **82,** 2979–2982.
8. Nicolelis, M. A. L., Baccala, L. A., Lin, R. C. & Chapin, J. K. (1995) *Science* **268,** 1353–1358.
9. Prechtl, J. C., Cohen, L. B., Mitra, P. P. & Kleinfeld, D. (1997) *Proc. Natl. Acad. Sci. USA* **94,** 7621–7626.
10. Contreras, D., Destexhe, A., Sejnowski, T. J. & Steriade, M. (1997) *J. Neurosci.* **17,** 1179–1196.
11. Chervin, R. D., Pierce, P. A. & Connors, B. W. (1988) *J. Neurophysiol.* **60,** 1695–1713.
12. Wadman, W. J. & Gutnick, M. J. (1993) *Neuroscience* **52,** 255–262.
13. Miles, R., Traub, R. D. & Wong, K. S. (1988) *J. Neurophysiol.* **60,** 1481–1496.
14. Traub, R. D., Jefferys, J. G. R. & Miles, R. (1993) *J. Physiol. (London)* **472,** 267–287.
15. Demir, R., Haberly, L. B. & Jackson, M. B. (1998) *J. Neurophysiol.* **80,** 2727–2742.
16. von Krosigk, M., Bal, T. & McCormick, D. A. (1993) *Science* **261,** 361–364.
17. Bal, T., von Krosigk, M. & McCormick, D. A. (1995) *J. Physiol. (London)* **483,** 641–663 and 665–685.
18. Steriade, M., McCormick, D. A. & Sejnowski, T. J. (1993) *Science* **262,** 679–685.
19. Kim, U., Bal, T. & McCormick, D. A. (1995) *J. Neurophysiol.* **84,** 1301–1323.
20. Golomb, D., Wang, X.-J. & Rinzel, J. (1996) *J. Neurophysiol.* **75,** 750–769.
21. Destexhe, A., Bal, T., McCormick, D. A. & Sejnowski, T. J. (1996) *J. Neurophysiol.* **76,** 2049–2070.
22. Rinzel, J., Terman, D., Wang, X.-J. & Ermentrout, B. (1998) *Science* **279,** 1351–1355.
23. Steriade, M., Domich, L., Oakson, G. & Deschênes, M. (1987) *J. Neurophysiol.* **57,** 260–273.
24. Bazhenov, M., Timofeev, I., Steriade, M. & Sejnowski, T. J. (1999) *Nat. Neurosci.* **2,** 168–174.
25. Thomson, A. M., Deuchars, J. & West, D. C. (1993) *J. Neurophysiol.* **70,** 2345–2369.
26. Markram, H., Lubke, J., Frotscher, M., Roth, A. & Sakmann, B. (1997) *J. Physiol. (London)* **500,** 409–440.
27. Tuckwell, H. C. (1988) *Introduction to Theoretical Neurobiology* (Cambridge Univ. Press, Cambridge).
28. Hansel, D., Mato, G. & Meunier, G. (1995) *Neural Comp.* **7,** 307–337.
29. Hansel, D., Mato, G., Meunier, C. & Neltner, L. (1998) *Neural Comp.* **10,** 467–483.
30. Chen, Z., Ermentrout, B. & Wang, X. J. (1998) *J. Comput. Neurosci.* **5,** 53–69.
31. Kim, U. & McCormick, D. A. (1998) *J. Neurosci.* **18,** 9500–9516.
32. Pinault, D. & Deschenes, M. (1998) *Eur. J. Neurosci.* **10,** 3462–3469.
33. Fleidervish, I. A., Binshtok, A. M. & Gutnick, M. J. (1998) *Neuron* **21,** 1055–1065.
34. Telfeian, A. E. & Connors, B. W. (1998) *Epilepsia* **39,** 700–708.
35. Markram, H. & Tsodyks, M. (1996) *Nature (London)* **382,** 807–810.
36. McKernan, M. G. & Shinnick-Gallagher, P. (1997) *Nature (London)* **390,** 607–611.
37. Saar, D., Grossman, Y. & Barkai, E. (1999) *J. Neurosci.*, **19,** 8616–8622.